7th International Symposium of Marine Propulsors
smp2022, Wuxi, China, October 17-21, 2022

Prediction of Underwater Radiated Noise from Propeller Cavitation During Concept Design

Frans Hendrik Lafeber, Johan Bosschers, Artur Lidtke, Thomas Lloyd, Erik van Wijngaarden, Joost Moulijn

Maritime Research Institute Netherlands (MARIN), Wageningen, The Netherlands

ABSTRACT

There is growing concern about the impact of underwater radiated noise (URN) on marine life. One of the main sources of URN of ships is propeller cavitation. Semi-empirical computational models to predict back (suction) side cavitation at the design point of open propellers have been published, but there is a lack of models that predict the URN of open propellers in off-design conditions and the URN of ducted propellers, such as thrusters. The European Union *NAVAIS*[1] project considered two ship types that spend large proportions of time operating at off-design conditions – a road ferry and an aquaculture workboat – and are therefore likely to experience several different forms of propeller cavitation. The present paper discusses new semi-empirical models to be used together with a boundary element method for predicting noise from these forms of cavitation. The new (medium-fidelity) models were tuned using data from a large series of model-scale noise measurements, supplemented by high-fidelity scale-resolving computational fluid dynamics simulations combined with the Ffowcs Williams-Hawkings acoustic analogy. The medium-fidelity models were used to predict the URN from a large series of propellers for a wide range of operating conditions, with the results used in a regression analysis to develop a low-fidelity tool for estimating propeller URN of road ferries and workboats during the concept design phase.

Keywords

Underwater radiated noise, propeller, cavitation, concept design

1 INTRODUCTION

Within the European Union-funded project *NAVAIS*, a modular approach for ship design and construction has been developed, which aims to minimise the environmental impact of new vessels. The emissions to air, such as CO_2 and SO_X, had to be reduced as much as possible compared to current similar vessels. In addition, their underwater radiated noise (URN) has to be minimised because of growing concern about the effect of URN on marine life (Duarte et al., 2021; Thomsen et al., 2021). Due to this increased awareness URN is specifically mentioned in Good Environmental Status (GES) Descriptor 11: "Energy incl. Underwater Noise" of the Marine Strategy Framework Directive (MSFD)[2]. Several classification societies are already offering "Quiet Class" notations to indicate that a ship has been designed to have low URN (Cruz et al., 2021), while a number of research projects dealing with prediction and mitigation of ship URN have been performed (e.g., AQUO, SONIC) .

Much of the work to date on predicting ship URN has looked at vessels operating around their design condition. While this covers the majority of the operational profile of many ship types, such as cargo vessels, some ship types spend more time at several different operating conditions. The *NAVAIS* project considered two ship types for which this is the case: a road ferry and an aquaculture workboat. Road ferries typically make relatively short transits meaning deceleration forms a large part of their operational profile and they are often equipped with controllable-pitch propellers. Both of these contribute to an increased chance of face-side cavitation occurring, which can lead to increased URN levels (Tani et al., 2016; Traverso et al., 2017; McIntyre et al., 2021). Workboats often make use of ducted propellers, which exhibit their own unique forms of cavitation, and spend a significant portion of their time operating at off-design conditions, including station keeping. Therefore, for these ship types (and others) it is important to be able to predict URN for a range of operating conditions.

To be able to do this during the concept design phase computationally-efficient numerical models are required. While model tests are the most accurate means of verifying URN performance, they are costly and require the detailed

[1] The *NAVAIS* project has received funding from the European's Horizon 2020 research and innovation programme (Contract No.: 769419)

[2] https://ec.europa.eu/environment/marine/good-environmental-status/descriptor-11/index_en.htm

geometry of a final design. Similarly, despite the increasing maturity of computational fluid dynamics (CFD) techniques for propeller noise prediction (Li et al., 2016), such methods remain prohibitive for design studies, for which large numbers of designs need to be evaluated. Therefore, mainly semi-empirical models are used during propeller design, such as the Empirical Tip Vortex (ETV) model of Bosschers (2018b). However, since this type of model also requires the ability to compute the propeller loading using a boundary element method (BEM), it is preferable to have an even simpler model for use in the early design phase, which only requires main ship and propeller particulars as input.

This paper details work performed to extend the ETV model to cover a number of additional forms of cavitation relevant for ferries and workboats, and the subsequent development of a low-fidelity URN model for concept design. The role of model test and high-fidelity CFD results in the development process is discussed.

2 APPROACH

Experiments (model tests) can be considered as the most accurate method available for design assessment before building the ship. However, this requires a physical model of the ship and propellers to be built and tested at the correct scaled conditions. One step lower is the high-fidelity approach of CFD, which can be combined with acoustic modelling to obtain an URN prediction. This negates the need to build a physical model but it still requires the detailed designs to be available, of which a high-quality computational grid needs to be created. Because of the high computational costs, such computations are (currently) only suited to design validation rather than design variations.

A medium-fidelity method such as the BEM PROCAL, combined with the ETV model (Bosschers, 2018b) is much faster than CFD computations. Rather than the days or even weeks of computational time required for CFD computations, each PROCAL + ETV computation takes only a few minutes. It still requires a detailed propeller design and the ship hull wake field as input. However, since it is quite fast, many different propeller designs can be evaluated in a short time.

Since PROCAL needs a wake field as input, it is generally used when main propeller parameters such as the propeller type and diameter have already been selected. These parameters have a big impact on ship design including URN. Therefore a low-fidelity tool, which uses a limited set of main design parameters to estimate the URN, can be useful to compare different ship concepts and propeller parameters. Such a tool typically runs very fast and can be used to explore many different concepts and to find suitable ranges of design parameters, which can be used as input or boundary conditions for the detailed design.

This sequence of decreasing fidelity was also followed in developing the low-fidelity models in the present work. Data from model-scale noise measurements has been combined with high-fidelity CFD computations to obtain data to extend and tune semi-analytical models. These newly developed models covered sheet cavitation and leading-edge vortex cavitation on both sides of the propeller, as well as tip-leakage vortex cavitation, which occurs in the gap between the propeller tip and the inside of the duct. The models were then combined with the ETV model, which was originally developed for tip vortex cavitation.

The new medium-fidelity models have been used in combination with PROCAL to compute the noise of many different propeller designs from the Wageningen C-, D- (Dang et al., 2013) and F-series (Huisman et al., 2021) at various operating conditions. By applying a regression analysis to the results of approximately 20,000 such computations, the low-fidelity models can be derived.

An overview of this approach from high-fidelity to low-fidelity is given in Figure 1.

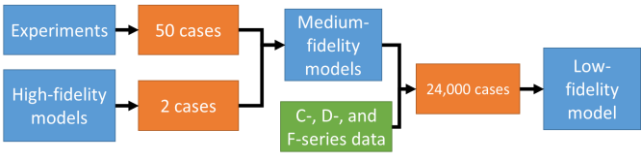

Figure 1: Overview of tool development approach (blue: developments within the *NAVAIS* project; green: data from other projects; orange: number of cases resulting from each approach.)

More details of each of the approaches shown in Figure 1 are given in the following sections.

3 EXPERIMENTS

A model test campaign was carried out to obtain noise data to tune the high-fidelity models and to validate the final noise estimation tool. Tests were performed for multiple propellers and operating conditions in MARIN's Depressurised Wave Basin (DWB).

3.1 Facility

The DWB measures 240 m long by 18 m wide and 8 m deep and the ambient pressure can be lowered to obtain the full-scale cavitation number in model-scale test conditions. The free water surface in this facility ensures that the pressure release boundary condition is satisfied. A dedicated silent towing carriage is used in the basin to minimise the disturbance of the measurements by background noise (Bosschers et al, 2013, Lafeber et al, 2015).

3.2 Test setup

The focus in the NAVAIS project was on double-ended ferries and workboats, which are both generally fitted with azimuthing thrusters in a pushing configuration. This means that the spatial distribution of the inflow velocity into the propeller (the wake field) is dominated by the thruster unit and not by the hull of the ship (as is the case for ships with propellers directly fitted to shafts). Therefore, a thruster setup (as shown in Figure 2 (a) and (b)) was selected for the model tests rather than a ship model since it adequately recreates both the workboat and ferry case. The main difference between the two is that workboats are usually fitted with ducted propellers to increase thrust and efficiency at low speeds while ferries typically use open propellers (without a duct), which are more efficient at higher speeds.

To ensure that there are sufficient nuclei to trigger cavitation on the propellers, electrolysis is used to generate small bubbles. A custom-made electrolysis system was developed for the tests, consisting of an array of three fins with metal strips glued to both sides, see Figure 2 (c). This array was fitted upstream of the thruster setup. To minimise the effect of the wake of the fins on the propeller, the middle fin was in line with the thruster strut while the two outer fins are just outside the propeller diameter. Figure 3 shows the entire setup in the DWB harbour area. The streamlined profile on the far right houses one of the high-speed video cameras used to observe the cavitation dynamics.

(a) Streamlined headbox

(b) Thruster housing, strut and transparent duct

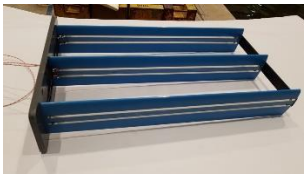

(c) Custom-made electrolysis fins

Figure 2: Photographs of various components of the test setup.

Figure 3: Test setup in the DWB harbour.

Two hydrophones were fitted to a mast on the centreline of the basin at approximately 1.2 m below the water surface. The signals from the hydrophones are sampled at 320 kHz with a low-pass filter at 100 kHz.

3.3 Test conditions

Two ducted propellers were tested: one without skew (Ka4-70) and one with skew (D4-70). A 19A duct has been used for both propellers. The ducted propellers were tested in both forward-speed and bollard-pull conditions. Three open propellers were tested, covering variations in pitch, number of blades and blade area ratio. One of them was tested at its design pitch and a reduced pitch to model low-speed sailing with a controllable-pitch propeller. The design pitch setting was $P_{0.7}/D = 1.0$ where $P_{0.7}$ is the pitch at 70 % of the propeller radius and D is the propeller diameter. The propeller operating conditions were defined in terms of the propeller advance ratio and cavitation number, given by

$$J_v = \frac{V}{nD} \tag{1}$$

and

$$\sigma_n = \frac{p_0 - p_v + \rho g h}{\frac{1}{2}\rho n^2 D^2}, \tag{2}$$

where V is the forward speed, n the rotation rate of the propeller, p_0 is the ambient pressure, p_v the vapour pressure, ρ the water density, g the gravitational acceleration, and h the immersion (depth of the propeller shaft is used here). The test conditions were chosen to cover a wide range of propeller loadings and cavitation numbers, in order to measure noise from different forms of cavitation. For the open propellers there was a focus on lightly-loaded conditions, corresponding to deceleration of ferries, while for the ducted propellers both station keeping (J_V = 0.0) and transit (J_V >> 0.0) conditions were simulated.

An overview of the different propellers and corresponding test conditions is shown in Table 1.

Table 1: Tested propellers and test conditions.

Propeller	Number of blades Z	Blade area ratio BAR	Pitch ratio $P_{0.7}/D$	Advance ratio J_V [-]	Cavitation number σ_n [-]
Ka4-70	4	0.7	1.0	0.00, 0.33-0.87	1.7-9.7
D4-70	4	0.7	1.0	0.00, 0.28-0.56	1.1-8.4
C4-70	4	0.70	1.0	0.93-1.24	1.5-6.4
C4-70	4	0.70	0.5	0.45-0.88	1.0-3.5
C4-55	4	0.55	1.0	0.87-1.47	1.6-6.5
C5-75	5	0.75	1.0	0.83-1.29	1.3-3.0

Measurements of the background noise – the total noise without cavitation present, which is needed to determine the signal-to-noise ratio (SNR) – were made at various test conditions albeit with a dummy hub without propeller blades.

3.4 Data analysis

The data analysis procedures applied for the measurements with forward speed followed those described by Lloyd et al. (2018), which can be broadly summarised as:

- window the signal symmetrically about the hydrophone position, limited to the reverberation radius in order to avoid reflections from the tank sides.
- segment the windowed data into 15 parts, with 50 % overlap.
- for each segment:
  - compute the power spectral density of the measured sound levels using Welch's method applying 50 % overlap.
  - derive source levels (SL) assuming spherical spreading loss and a correction for the Lloyd's mirror effect due to the free surface.
  - compute broadband levels by apply one-third octave (OTO) filtering.
  - perform a SNR correction using (non-cavitating) background noise measurement data for each (cavitating) OTO data point, following ITTC (2017).
- average the resulting background-noise corrected source levels over all 15 segments to derive the final OTO source level spectrum. For OTO frequencies in which the SNR was not sufficient for more than half of the segments, the averaged data point is omitted.

Analysis of stationary tests followed a similar procedure without the need to window and segment the data, since the distance between the propeller and hydrophone was fixed, and within the measured reverberation radius of the DWB (Lafeber et al, 2015).

3.5 Results overview

Analysed sound levels of two cases are given in Figure 4 and Figure 5, in the form of OTO source level spectra for cavitating propeller and dummy hub configurations.

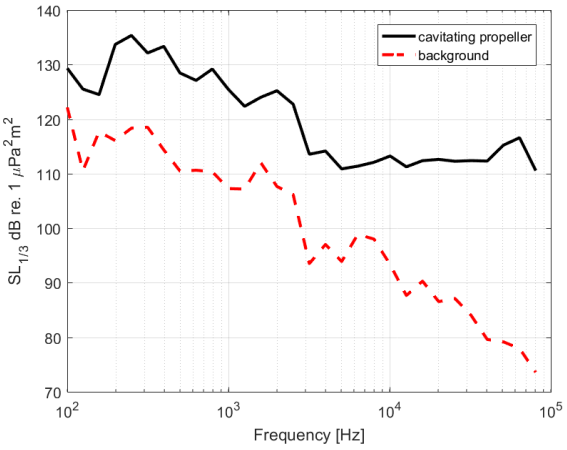

Figure 4: Sound source levels of ducted propeller in bollard-pull condition.

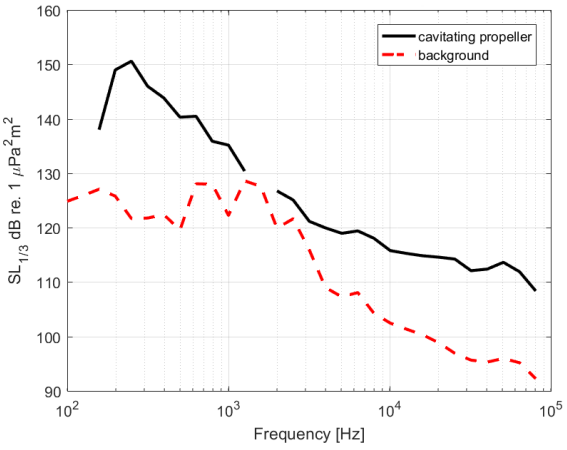

Figure 5: Sound source levels of open propeller in near-zero thrust condition.

The SNR is sufficient at almost all frequencies for both cases shown here. Only for the open propeller a couple of data points between 1 and 2 kHz have been removed during the analysis, which does not compromise interpretation of

the overall spectral form. This makes the results shown suitable as comparison for numerical results, as well as for use in deriving the medium-fidelity models.

4 HIGH-FIDELITY MODEL

4.1 Methodology

Detailed CFD simulations have been carried out to obtain information about the leading-edge vortex strength and size, for propeller C4-70 with$P_{0.7}/D$= 0.5, J_V= 0.455, σ_n=2.50. Numerical prediction of the flow was carried out using the viscous CFD code, ReFRESCO, developed by MARIN in collaboration with various institutes and universities worldwide, in order to provide a flow solver specifically tailored to maritime applications. In the code, the incompressible Navier-Stokes equations are solved in a segregated manner. Cavitation is modelled using a single-phase approach based on the Schnerr & Sauer (2001) model. Model constants were set based on prior experience and are the nuclei radius, R_0 = 10 μm, and population density, $n_0 = 10^8$ m^{-3}. The model has seen significant use and validation (Vaz et al., 2015; Liebrand et al., 2021; Lidtke et al., 2019) and is considered as a robust numerical approach suitable for engineering applications.

Accurate capture of the face-side cavitating vortex also necessitated the use of a scale-resolving turbulence model. This was required in order to reduce the numerical dissipation allowing the low pressure at the vortex core to be better resolved than with standard Reynolds-averaged Navier-Stokes (RANS) turbulence models. Due to the relatively high Reynolds numbers involved in the present study, improved detached eddy simulation (IDDES), introduced by (Gritskevich et al., 2012), was used. This allows turbulence to be resolved away from the propeller surface, capturing unsteady vortex and cavitation dynamics, but utilises RANS close to the wall. This reduces the grid density requirements compared to full large eddy simulation (LES) and is hence more computational efficient.

For predicting URN the Ffowcs Williams Hawkings (1969) acoustic analogy was applied, in which a so-called ‘porous data surface’ is placed around the noise sources - described by the incompressible flow solution – which are propagated to far field receivers analytically. A more in-depth description of the simulations is given by Lidtke et al. (2022).

4.2 Test case set up

At the chosen grid size, 26.5 million cells were used for the baseline grid of the propeller and the encompassing domain. At this refinement level, the discretisation uncertainty of thrust, torque and duct thrust force coefficients were estimated to be approximately 4 %. In order to allow better resolution around the face side vortex forming along the leading edge of the propeller, adaptive grid refinement was subsequently included in the computations, increasing the cell count to 56.7 million cells. The grid was designed to satisfy the $y+ < 1$ criterion for wall-normal cell size. Additionally, between 10 and 20 cells were present across the vortex viscous core diameter with local variations due to exact vortex size, position, and specific refinement criteria used. The chosen domain size corresponded to the cross-section of the DWB with a length of 9 m in order to prevent the accelerated flow behind the propeller from reflecting from the domain outlet and affecting the results upstream.

A Dirichlet boundary condition for velocity and the turbulence model quantities was specified at the inlet, with a Dirichlet condition for pressure used at the top of the domain. The bottom and sides of the domain were modelled as slip walls. The outlet was modelled using a Neumann boundary condition.

The simulations were run for twenty propeller revolutions, applying progressively finer time steps until the last six revolutions, for which a fixed time step equivalent to 0.2 degrees of propeller rotation was used. Both wetted (cavitation model switched off) and cavitating flow conditions were simulated, in order to be able to determine the numerical SNR.

4.3 Vortex analysis

In order to provide data necessary for the development of the medium-fidelity model, vortex trajectory had to be traced in the simulation and its properties extracted. This was done by defining a number of circular slices through the domain along the expected vortex trajectory, estimated using the geometric pitch of the propeller. This is depicted in Figure 6. Data were extracted for a single time step corresponding to the blade in the top position and on each slice a vortex identification algorithm using velocities in the plane normal to the expected vortex trajectory (Phillips & Turnock, 2013) was applied . The results were also compared with the location of maximum vorticity in the direction parallel to the vortex core and location of minimum pressure on each slice. In cavitating conditions, the geometric centroid of the cavity was taken as the vortex core position. Once the centre of the vortex has been found, tangential velocity profiles could be extracted from the CFD results and regressed using the Scully empirical vortex model (see Bosschers (2018)). With this information, a full analytical description of the vortex could be constructed and used in the empirical model. The computed circulation is depicted in Figure 7.

The identified vortex trajectory may also be plotted together with the CFD results, as shown in Figure 8, in order to better explain the mechanisms leading up to the formation of the face-side vortex. In non-cavitating

conditions, the vortex appears around mid-span of the blade. A contra-rotating vortex then develops further along the blade and passes over the tip. When cavitation is included in the simulation, a clearly identifiable cavity may be seen along almost the complete span of the blade. Around the inception location, the cavity may be classified as an attached sheet, which then rolls up into the main vortex and carries on along its core. The cavitating vortex then separates from the blade at around mid-chord. Another point to note is that the cavitating vortex trajectory differs from the non-cavitating one.

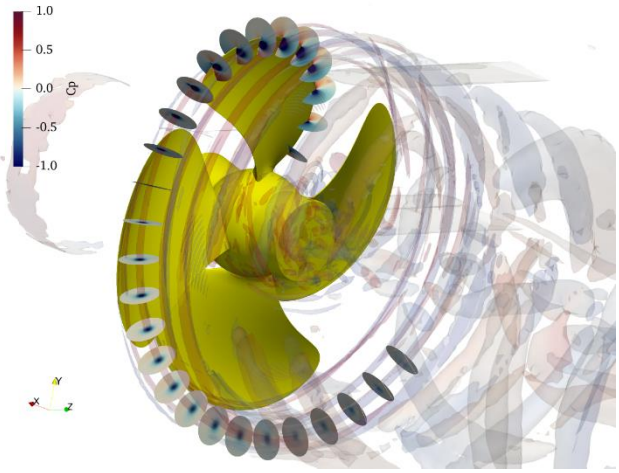

Figure 6: Q-criterion iso-contour around the propeller and circular planes used to precisely identify the vortex trajectory; coloured by pressure coefficient based on propeller diameter and rotation rate.

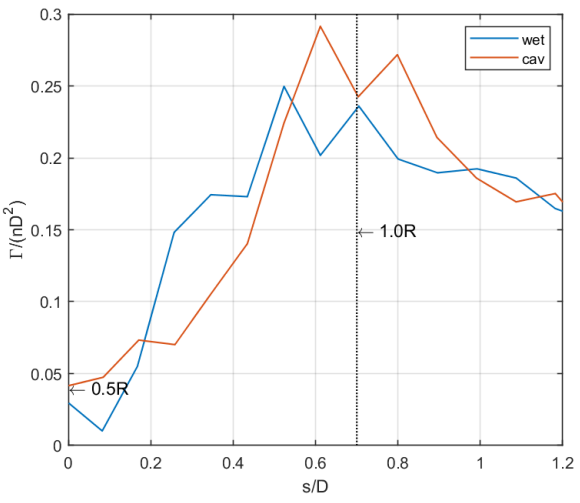

Figure 7: Vortex strength (Γ) non-dimensionalised by propeller rotation rate and propeller diameter at various positions along the vortex core. Distance *s* denotes the distance along the vortex trajectory. "Wet" and "cav" refer to wetted and cavitating conditions, respectively.

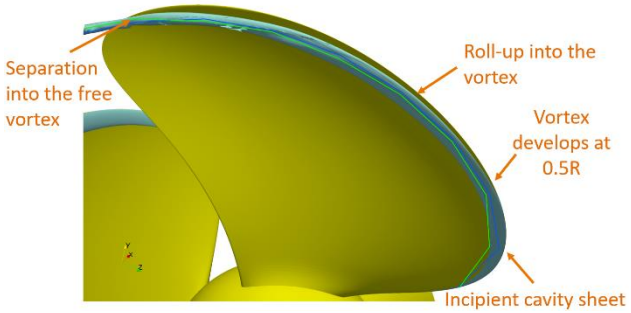

Figure 8: Cavitating (blue) and non-cavitating (green) vortex path relative to cavity iso-contour.

5 MEDIUM-FIDELITY MODELS

For the development of the medium-fidelity noise prediction, use was made of the BEM PROCAL, developed by MARIN within the Cooperative Research Ships[3] (CRS) for the unsteady analysis of cavitating propellers operating in a prescribed ship wake field. It has been validated for open water characteristics, shaft forces and moments, sheet cavitation extents and propeller-induced hull-pressure fluctuations. The code is a low-order BEM that solves for the velocity disturbance potential using the Morino formulation. Initial validation studies and details on the mathematical and numerical model are described by Vaz (2005) and Vaz and Bosschers (2009). The geometry of the blade wake can be determined by an iterative procedure to align the propeller wake with the flow or by using a prescribed wake pitch and contraction using empirical formulations to reduce CPU time. For the analysis of ducted propellers, an iterative wake alignment method is used for the wake of the propeller and duct in which the radial position of the trailing vortices is prescribed while the pitch is obtained from the computed induced velocities. The duct trailing edge geometry is modified such that a sharp trailing edge is present and the location from which the vortices trail from the duct is clearly defined. An iterative pressure Kutta condition is applied in which the duct and propeller wake strength is modified until the pressure difference on the two surfaces at the trailing edge of blade and duct is smaller than a user specified value (Bosschers et al. 2015). Results of PROCAL for ducted propellers are also presented by Moulijn et al. (2019).

The broadband URN of cavitating propellers is currently predicted using semi-empirical models for cavitating tip vortices (Bosschers, 2018a, 2018b) and sheet cavitation (Brown, 1999). These models are based on the vortex cavity diameter estimated from the propeller blade tip loading computed by PROCAL together with an analytical vortex model, and on the maximum sheet cavity area directly predicted by PROCAL. These cavity extents determine the maximum source level and corresponding frequency through empirical factors, from which the

[3] www.crships.org

broadband source level spectrum is obtained using an assumed spectral shape.

A similar approach has been used for the development of the new noise models, making use of a non-dimensional pressure coefficient K_p, expressed in decibels as

$$K_p\left(f/f_{bp}\right)=10\log_{10}\left[\frac{p'^2\left(f/f_{bp}\right)/p_{ref}^2}{\rho^2 n^3 D^6}\right] \qquad (3)$$

where p'^2 is the power spectral density of the sound pressure in $\left[\mathrm{Pa}^2/\mathrm{Hz}\right]$ at 1 m distance and p_{ref} is the reference pressure, which is taken as $p_{ref}=1\mu\mathrm{Pa}$. The frequency f is normalised using the blade passage frequency f_{bp}.

The experimental data was non-dimensionalised using this approach for further analysis. Cases for which only one particular kind of cavitation was present were used for the development of the new URN models, with each case computed using PROCAL. Example panel distributions used for the PROCAL computations are given in Figure 9. These panels were generated using the computer code PROVISE, developed by DRDC Atlantic for CRS.

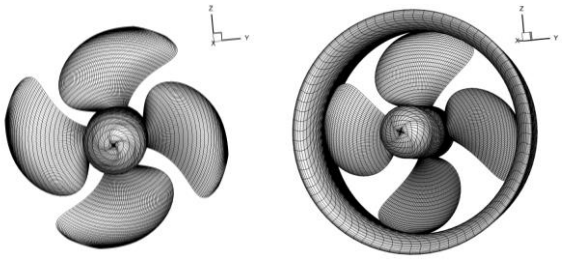

C4-70, $P_{0.7}/D$ = 0.5 D4-70, $P_{0.7}/D$ = 1.0 in 19A duct

Figure 9: Examples of the PROCAL panel distributions.

Two types of cavitation were distinguished for the development of the semi-empirical models, namely a sheet cavity and a vortex cavity. For both cavity types, a formulation for the maximum value of K_p and its frequency was derived. In combination with a prescribed spectral shape, the variation of K_p with frequency is obtained.

For sheet cavitation, the generic semi-empirical formulation for $K_{p,max}$ reads:

$$K_{p,max}=c_{s1}+10\log_{10}\left\{Z\left(\frac{A_{cav,max}}{A_0}\right)^{c_{s2}}\right\}, \qquad (4)$$

with $A_{cav,max}$ the maximum sheet cavity area on the propeller blade during a revolution, A_0 the propeller disc area, and c_{s1} and c_{s2} the empirical constants. The prediction of the area of sheet cavity by PROCAL was found to be more robust than the prediction of the cavity volume and its time derivatives. Following Brown (1999), the spectral shape consists of a plateau at low frequency changing into a decay with constant slope above frequency f_p. The maximum frequency of the plateau is given by

$$\frac{f_p}{f_{bp}}=c_{s3}\frac{\sqrt{\sigma_n}}{\left(A_{c,max}/A_0\right)Z}. \qquad (5)$$

The formulation for K_p is then given by

$$K_p\left(f/f_{bp}\right)=K_{p,max}+10\log_{10}\left[\left(\frac{\max\left(f/f_{bp},f_p/f_{bp}\right)}{f_p/f_{bp}}\right)^{-2.0}\right]. \qquad (6)$$

For back-side sheet cavitation, the values for the empirical coefficients were taken from Brown (1999), whereas for face-side sheet cavitation new values were derived from the model-scale measurements for which further details are provided later in this section.

For a vortex cavity, the generic semi-empirical formulation for $K_{p,max}$ reads:

$$K_{p,max}=c_{v1}+10\log_{10}\left\{Z\left(\frac{r_c}{D}\right)^{c_{v2}}\right\} \qquad (7)$$

with c_{v1} and c_{v2} the empirical constants, Z the number of propeller blades, and r_c/D the vortex cavity radius made non-dimensional with the propeller diameter. The vortex cavity radius is computed using a Rosenhead vortex model assuming that the cavity radius equals the radius of the non-cavitating vortex at which pressure equals vapour pressure (Bosschers, 2018a). The advantage of the Rosenhead vortex model is that the cavity radius can be computed using a simple analytical relation involving maximum vortex strength Γ_∞ and cavitation number σ_n (from which the inviscid cavity size $\left(r_c/D\right)_{inv}$ can be computed) and viscous core size r_v:

$$\left(r_c/D\right)_{inv}=\left(\frac{1}{2\pi}\right)\left(\frac{\Gamma_\infty}{nD^2}\right)\frac{1}{\sqrt{\sigma_n}} \qquad (8)$$

$$\left(r_c/D\right)=\sqrt{\max\left\{0,\left(r_c/D\right)_{inv}^2-\left(r_v/D\right)^2\right\}} \qquad (9)$$

The value for r_v is taken from reference data measured at model scale, combined with a Reynolds number scaling. The spectral shape contains a hump at low frequency with a constant slope at high frequencies, similar to the tip-vortex cavity model proposed by Bosschers (2018b). The non-dimensional centre frequency of the hump is given by

$$\frac{f_c}{f_{bp}}=c_{v3}\frac{1}{r_c/D}\frac{\sqrt{\sigma_n}}{Z} \qquad (10)$$

Further details on the procedure for fitting the empirical parameters for tip-vortex cavitation, leading-edge vortex cavitation, and tip-leakage vortex cavitation are given later in this section.

Face-side sheet cavitation

The radiated noise measurements with sheet cavitation on the face of the propeller were not well described by the model of Brown (1999) and a new fit was made for the dependency of K_p on the maximum sheet cavity area as discussed above.

The model was tuned using the data of the open propeller C4-55 ($P_{0.7}/D$ = 1.0) at various cavitation numbers and thrust coefficients K_T, which is defined as

$$K_T = \frac{T}{\rho n^2 D^4} \tag{11}$$

An example of the cavitation extent as observed in the DWB and as computed by PROCAL is shown in Figure 10 and Figure 11. The fit of the experimental data is presented in Figure 12.

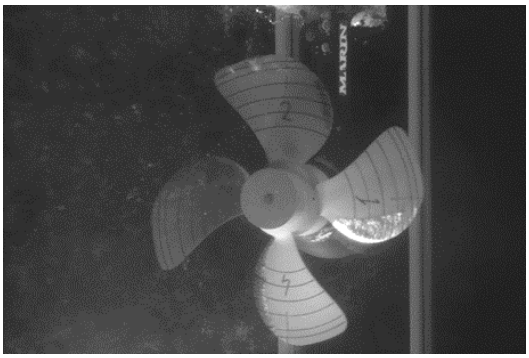

Figure 10: Face-side sheet cavitation, propeller C4-55, $P_{0.7}/D$ = 1.0, model test, K_T = 0.06, σ_n = 1.70.

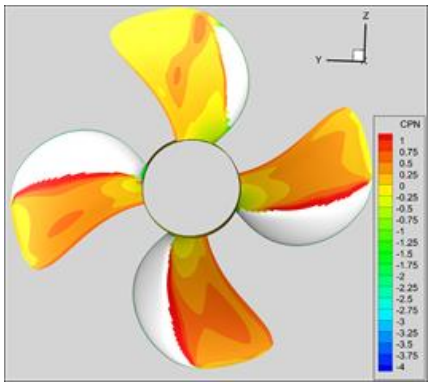

Figure 11: Face-side sheet cavitation, propeller C4-55, $P_{0.7}/D$ = 1.0, PROCAL sheet cavity extents and pressure distribution, K_T = 0.06, σ_n = 1.70.

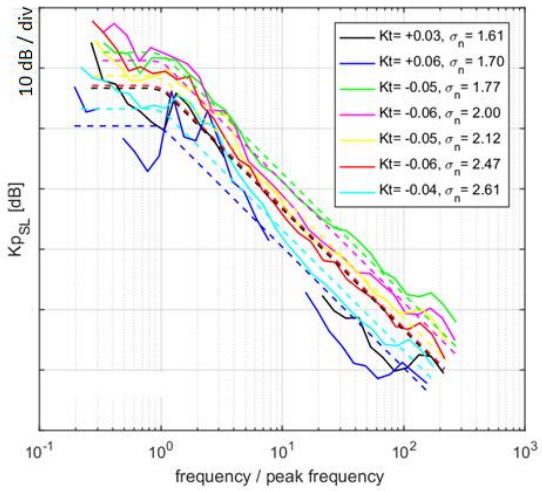

Figure 12: Face-side sheet cavitation, propeller C4-55, $P_{0.7}/D$ = 1.0, measured (solid line) and fitted (dashed line) non-dimensional sound spectrum.

Tip-vortex cavitation

The tip-vortex cavitation model is based on the model described in Bosschers (2018b), with small modifications were made due to the slightly different definition of K_p. Furthermore, the Rosenhead vortex model has been used rather than the Proctor vortex model in order to easily separate the potential flow effect from the viscous flow effect on the vortex cavity size. The spectral shape is similar to that of Bosschers (2018b), being characterised by a low-frequency hump in combination with a high-frequency slope. The model was tuned using the same experimental data set as used in Bosschers (2018b).

Face-side leading-edge vortex cavitation

For the face-side leading edge vortex cavitation model a similar form to the tip-vortex cavitation model was assumed. The vortex strength is computed in PROCAL using the theory by Polhamus (1966), which states that the strength of the leading edge vortex can be computed by potential flow theory from the leading-edge suction force. For rounded leading-edge sections, a correction needs to be applied for the nose drag which depends on the leading-edge curvature (Kulvan, 1979). To simplify the formulation in PROCAL, a single reference value for the leading-edge vortex strength was used by integrating the leading-edge suction force from the propeller radius where it becomes different from zero until the non-dimensional radius of 0.95. The latter was used to improve robustness. The PROCAL-predicted leading-edge vortex strength and viscous core radius were tuned using the IDDES computations presented in Section 4. The experimental data for propeller C4-70, $P_{0.7}/D$ = 0.5 for thrust coefficients near zero and varying cavitation numbers were used to tune the coefficients for the hump centre frequency

and its non-dimensional source level. The non-dimensional spectra show a very weak dependency on cavitation number, which is currently not understood.

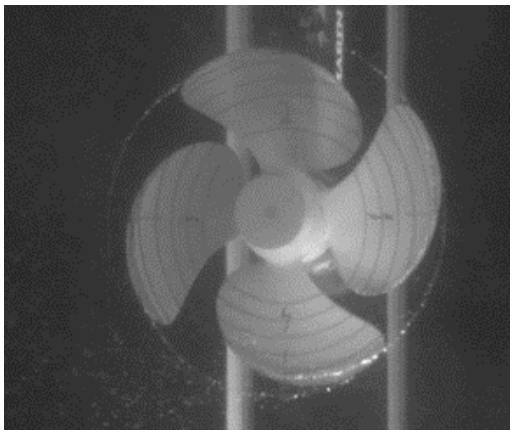

Figure 13: Face-side leading-edge cavitation, propeller C4-70, $P_{0.7}/D$= 0.5, model test, K_T = -0.02, σ_n = 3.00

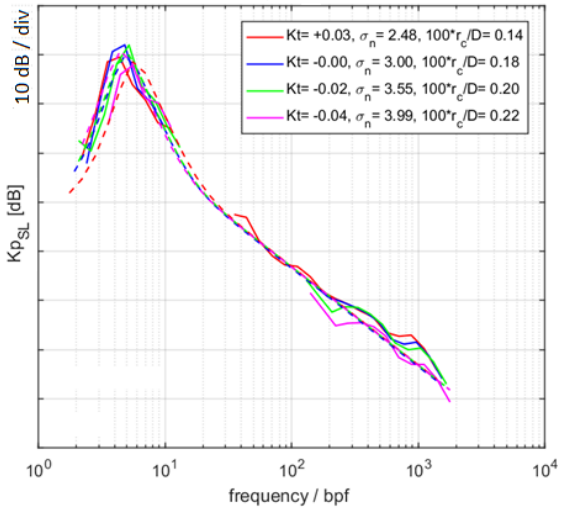

Figure 14: Face-side leading-edge cavitation, propeller C4-70, $P_{0.7}/D$= 0.5, measured (solid line) and fitted (dashed line) non-dimensional sound spectrum

Tip-leakage vortex cavitation

For ducted propellers, the formulation for the tip-vortex cavitation is replaced by the formulation for tip-leakage vortex cavitation. In PROCAL, the gap between the propeller and the duct is also modelled by panels following Baltazar et al. (2012). The tip-leakage vortex strength is computed from the normal force coefficient of the gap for which the gap discharge coefficient is set to zero. So far, only a tip-leakage vortex on the back of the propeller has been analysed. The reference values of the vortex viscous core size were taken from Oweis et al. (2006) and the Reynolds number scaling of the viscous core from the 21st ITTC Cavitation Committee (1996). The spectral shape was assumed to be the similar to that of sheet cavitation, but it is remarked that this choice was not very obvious and that some cases do suggest the presence of a hump. This requires further investigation. The fit has been performed for propellers Ka4-70 and D4-70 for cases for which no sheet cavitation was present. The model tests for the Ka4-70 also showed a thin cavitating hub vortex of which the contribution to the underwater radiated noise was assumed negligible.

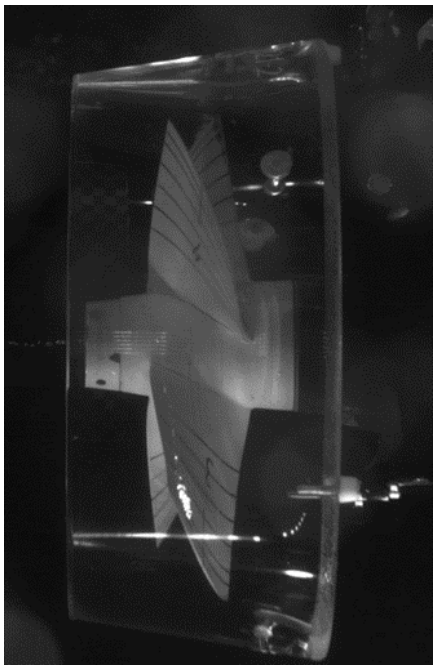

Figure 15: Tip-leakage vortex cavitation, propeller Ka4-70, K_T = 0.15, σ_n = 2.32.

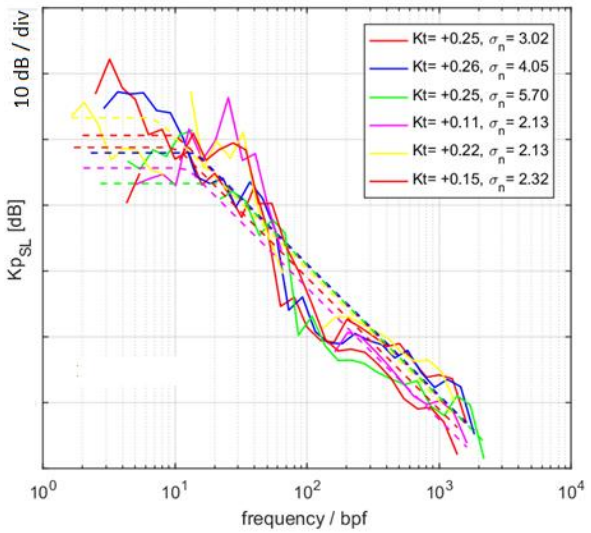

Figure 16: Tip-leakage vortex cavitation: measured (solid line) and fitted (dashed line) non-dimensional sound spectrum. Selected runs for propeller D4-70 propeller (first three cases) and Ka4-70 (last three cases).

6 LOW-FIDELITY MODELS

As discussed in Section 2, a regression-based low-fidelity model is needed to assist ship and propeller designers in an early design phase. However, it is impractical to create a regression model that makes use of complete noise spectra, which are arrays of values rather than a single value. Therefore, the low-fidelity models are based on either cavitation area (for sheet cavitation) or vortex strength in terms of circulation (for tip vortex, leading-edge vortex, and tip-leakage vortex cavitation). The estimated values for these quantities can then be used to construct the noise spectrum using the medium-fidelity models.

The input for the models was a large series of propeller computations. The sheet cavitation area and vortex strengths have been computed for a large range of propeller designs taken from the Wageningen C-, D- and F-series (see Figure 17), at various operating conditions. In total approximately 24,000 such computations were carried out.

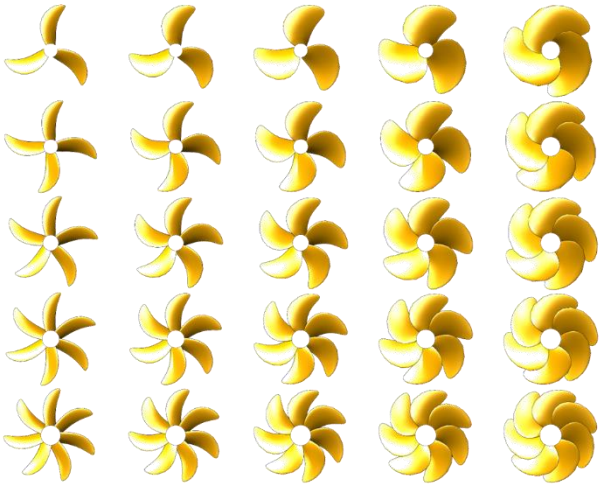

Figure 17: Impression of various propeller designs from the Wageningen F-series used in deriving the low-fidelity models.

The computed cavity areas and vortex strengths – for each cavitation type and on both face side and back side of the propeller – were used as a target in non-linear regression methods. The significant input parameters were determined for each cavitation type individually.

The low-fidelity models require some information about the ship e.g. number of propellers and draught (to compute the cavitation number), the propeller e.g. diameter, number of blades, pitch, and the operating conditions e.g. thrust, propeller rotation rate. An overview of the required input per regression-based model is shown in Table 2. The number of input parameters is quite limited. Several parameters were found not to be significant in the regression analysis. Some parameters were not varied in the aforementioned large series of propeller computations, because no large deviations occur in practice. One such parameter is the distance between the tip of a ducted propeller and the inside of the duct; that was kept constant at the industry standard of 1 % of the propeller diameter for all computations.

The cavitation area A_C is the ratio between the area covered by sheet cavitation and the propeller disk area, P_{tip} the pitch at the tip of the propeller and S_{LE} the skew angle at the leading edge.

The input consists of only a single propeller/ship design but a range of operating conditions can be supplied in the input files (including changes in pitch setting). The noise for each operating condition is then computed. Since the regression models only give the cavitation area and vortex strength, an additional step to obtain the noise levels is needed. The extended ETV-model (see Section 5), with the new medium-fidelity models, is used for this step. Rather than using the cavitation parameters obtained from a PROCAL computation, the output of the regression model is used as input for the ETV-model.

Table 2: Input parameters for low-fidelity models to predict the non-dimensional URN source levels (K_P-spectrum)

Cav. type	Applicability	Input	Output
Sheet	Face + back, open + ducted propellers	σ_n, K_T, Z, BAR, $P_{0.7}/D$	Cavitation area A_C
Tip-vortex	Face + back, open + ducted propellers	J_V, K_T, Z, BAR, P_{tip}/D	Vortex strength Γ
Leading-edge	Face + back, open propellers	J_V, K_T, Z, BAR, P_{tip}/D, S_{LE}	Vortex strength Γ
	Back, ducted propellers	J_V, K_T, BAR, S_{LE}	
	Face, ducted propellers	J_V, K_T, S_{LE}	
Tip-leakage vortex	Face, ducted propellers	J_V, P_{tip}/D	Vortex strength Γ

The process of collecting input, computing cavitation parameters with low-fidelity models, and computing the resulting noise spectra has been implemented in a software programme named “Aurras”. Results are graphically presented and compared to URN noise limits as specified by the class societies. The initial design parameters can be changed in the user interface of Aurras. By modifying these and calculating the new, corresponding, noise levels, a designer can quickly iterate between designs, and thus find propeller design parameters that lead to sufficiently low noise levels. However, changing some of the propeller parameters will also influence the required propeller rotation rate and the propeller efficiency. Ideally, those quantities should be computed again for the updated

propeller design and used as input for a new noise estimation. At this moment, this iterative process – including updating the propeller performance – is not yet implemented.

An Aurras computation has been performed for one of the cases of the experimental campaign (see Section 3): the C4-55 open propeller at a pitch setting of $P_{0.7}/D$ = 1.0. The thrust coefficient in this test was almost zero to model deceleration of the vessel. This condition resulted in mainly sheet cavitation on the face side of the propeller. A comparison of the Aurras result with that from the model tests is shown in Figure 18.

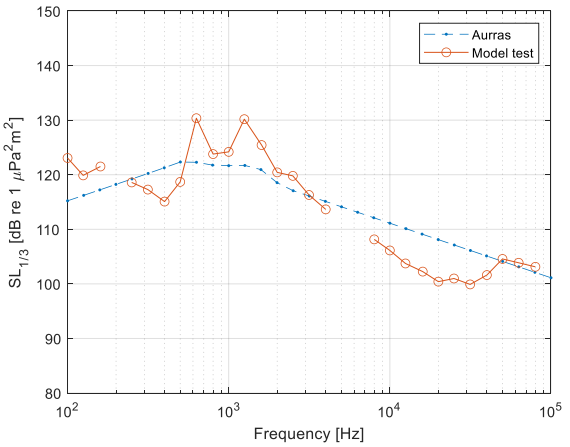

Figure 18: Comparison of Aurras result with model test result for C4-55 propeller

The noise levels are generally well predicted with the main hump also centred at the correct frequency. Not only are details of the noise spectrum well captured but the results are acceptable for use in an early design phase. Other cases showed similar results.

Since Aurras is a low-fidelity model, it only gives an indication of the noise levels based on a few parameters. More detailed computations, for example with the medium-fidelity models, should be done to validate a specific propeller design at specific operating conditions. In those computations, the influence of hull form design (wake field) is also taken into account, contributing to a more accurate prediction.

7 CONCLUDING REMARKS

A URN prediction tool has been developed for application in the early design phase of ferries and workboats. The tool is based on low-fidelity models derived from a regression analysis of a large number of computations using (medium-fidelity) semi-empirical models. Those models were also derived as part of the present study, making use of results from dedicated model tests and high-fidelity CFD computations.

The models distinguish between various types of cavitation relevant for ferries and workboats, such as tip-vortex cavitation, back- and face-side sheet cavitation, leading-edge face-side cavitation and tip-leakage vortex cavitation. Overall, an acceptable agreement between the various models could be obtained.

The low-fidelity model only requires main propeller particulars as input and is specifically developed for wake fields of a thruster. In principle, the models can be extended to model propellers operating in a wake field as well.

The approach is based on non-dimensional formulations of the sound source levels which worked well. However, the non-dimensional spectra of leading-edge vortex cavitation on the face side of the propeller showed a very low dependency on cavitation number and propeller loading which was not understood and needs to be further investigated. Furthermore, the models for the specific cavitation types still need to be validated using full-scale data which was not performed in the present project due to lack of data.

ACKNOWLEDGEMENTS

Funding for the *NAVAIS* project (Contract No.: 769419) from the European Union Horizon 2020 programme is gratefully acknowledged. We would also like to thank our colleagues at MARIN who helped in preparing and performing the model tests, and our colleague Mircea Pitigoi who developed the Aurras software.

REFERENCES

Baltazar, J., Falcao de Campos, J.A.C., and Bosschers, J. (2012). 'Open-water thrust and torque predictions of a ducted propeller system with a panel method', International Journal of Rotating Machinery, Volume 2012. https://doi.org/10.1155/2012/474785.

Bosschers, J., Lafeber, F.H., de Boer J., Bosman, R., Bouvy, A., 2013. 'Underwater radiated noise measurements with a silent towing carriage in the Depressurized Wave Basin', Proceedings of the 3rd International Conference on Advanced Model Measurement Technology, Gdansk, Poland.

Bosschers, J., Willemsen, C., Peddle, A., Rijpkema, D. (2015). 'Analysis of ducted propellers by combining potential flow and RANS methods'. Proceedings of the 4th International Symposium on Marine Propulsors, Austin, USA.

Bosschers, J., (2018a). 'Propeller tip-vortex cavitation and its broadband noise'. PhD thesis, University of Twente, Enschede, the Netherlands.

Bosschers, J. (2018b). 'A semi-empirical prediction method for broadband hull pressure fluctuations and underwater radiated noise by propeller tip vortex cavitation'. Journal of Marine Science and

Engineering 6(49). https://doi.org/10.3390/jmse6020049.

Bosschers, J., Vaz, G., Starke, A.R., van Wijngaarden, E. (2008). 'Computational analysis of propeller sheet cavitation and propeller-ship interaction'. In Proceedings of the RINA MARINE CFD Conference, Southampton, UK.

Brown, N.A. (1999). 'Thruster noise'. Proceedings of the Dynamic Positioning Conference of the Marine Technology Society, Houston, USA.

Cruz, E. Lloyd, T., Bosschers, J., Lafeber, F.H., Vinagre, P. Vaz, G., (2021). 'Study on inventory of existing policy, research and impacts of continuous underwater noise in Europe.' EMSA report EMSA/NEG/21/2020. WavEC Offshore Renewables and Maritime Research Institute Netherlands.

Dang, J., van den Boom, H.J.J., Ligtelijn, J.Th., 2013 'The Wageningen C- and D-Series propellers', 12th International Conference on Fast Sea Transportation, Amsterdam, the Netherlands.

Duarte, C. M., Chapuis, L., Collin, S. P., Costa, D. P., Eguiluz, V., Erbe, C., Halpern, B. S., Havlik, M. N., Gordon, T. A. C., Merchant, N. D., Meekan, M., Miksis-Olds, J. L., Parsons, M., Predragovic, M., Radford, A. N., Radford, C. A., Simpson, S. D., Slabbekoorn, H., Staaterman, E., Opzeeland, I.C., Van Winderen, J., Zhang, X. and Juanes, F. (2021). The soundscape of the anthropocene ocean. Science, 371(6529). https://doi.org/10.1126/science.aba4658.

Ffowcs Williams, J.E., Hawkings, D.L., 1969. Sound generation by turbulence and surfaces in arbitrary motion. Philosophical Transactions of the Royal Society A: Mathematical, Physical and Engineering Sciences 264, 321–342. doi:10.1098/rsta.1969.0031.

Gritskevich, M.S., Garbaruk, A.V., Schutze, J., Menter, F.R., 2012. Development of DDES and IDDES formulations for the k-w shear stress transport model. Flow, Turbulence and Combustion 88, 431–449. https://doi.org/10.1007/s10494-011-9378-4.

Huisman, J., Foeth, E.-J., Slot, J., Lampe, A., Moulijn, J., Dang, J., Design of the Wageningen F-Series, working paper, MARIN, April 2021, Wageningen, the Netherlands (https://www.marin.nl/en/news/working-paper-on-the-design-of-the-wageningen-f-series, accessed 11th July 2022).

ITTC (2017) 'Recommended procedures and guidelines. Model-scale propeller cavitation noise measurements', *7.5-02-01-05*, International Towing Tank Conference, Zurich, Switzerland.

Kulfan, R.M. (1979). 'Wing geometry effects on leading-edge vortices'. AIAA Aircraft systems and technology meeting, AIAA paper no. 78-1872, New York, USA.

Lafeber, F. H., Bosschers, J. B., de Jong, C. and Graafland, F., 2015. 'Acoustic reverberation measurements in the Depressurised Wave Basin', in: Proceedings of the 4th International Conference on Advanced Model Measurement Technology, Istanbul, Turkey.

Li, D.-Q., Hallander, J. and Johansson, T. (2016) Predicting underwater radiated noise of a full scale ship with model testing and numerical methods. Ocean Engineering, 161, 121-135. https://doi.org/10.1016/j.oceaneng.2018.03.027.

Liebrand, R., Klapwijk, M., Lloyd, T., Vaz, G., 2021. Transition and turbulence modeling for the prediction of cavitating tip vortices. Journal of Fluids Engineering 143, 011202–1 – 011202–14. https://doi.org/10.1115/1.4048133.

Lidtke, A.K., Lloyd, T., Vaz, G., 2019. Acoustic modelling of a propeller subject to non-uniform inflow, in: Proceedings of the 6th International Symposium on Marine Propulsors, Rome, Italy.

Lidtke, A.K., Lloyd, T., Lafeber, F.H., Bosschers, J., 2022. 'Predicting cavitating propeller noise in off-design conditions using scale-resolving CFD simulations'. Ocean Engineering 254, 111176. https://doi.org/10.1016/j.oceaneng.2022.111176.

Lloyd, T., Lafeber, F.H., Bosschers, J., 2018. 'Investigation and validation of procedures for cavitation noise prediction from model-scale measurements', 32nd Symposium on Naval Hydrodynamics, Hamburg, Germany.

McIntyre, D., Lee, W., Frouin-Mouy, H., Hannay, D. and Oshkai, P. (2021) Influence of propellers and operating conditions on underwater radiated noise from coastal ferry vessels. Ocean Engineering, 232, 109075. https://doi.org/10.1016/j.oceaneng.2021.109075.

Moulijn, J., Bosschers, J., Tornros, S., Schreiber, C., Grassi, D., Goedbloed, I., Bijlard, M. (2019). 'Validation studies of a boundary element method for ducted propellers'. Proceedings of the 6th International Symposium on Marine Propulsors, Rome, Italy.

Oweis, R.F., Fry, D., Chesnakas, C.J., Jessup, S.D., Ceccio, S.L. (2006). 'Development of a tip-leakage flow - part 1: The flow over a range of Reynolds numbers'. Journal of Fluids Engineering, v. 128(4), p. 751-764.

Phillips, A.B. and Turnock, S.R., 2013. Application of the VORTFIND algorithm for the identification of vortical flow features around complex three-dimensional geometries. International Journal for Numerical Methods in Fluids, 71(11), pp.1461-1474.

Polhamus, E.C. (1966). 'A concept of the vortex lift of sharp-edge delta wings based on a leading-edge suction analogy'. NASA TN D-3767.

Sauer, J., Schnerr, G.H., 2001. Development of a new cavitation model based on bubble dynamics. Zeitschrift fur Angewandte Mathematik und Mechanik 81, 561–562. doi:10.1002/zamm.20010811559.

Tani, G., Viviani, M., Hallander, J., Johansson, T. and Rizzuto, E. (2016) Propeller underwater radiated noise: A comparison between model scale measurements in two different facilities and full scale measurements. Applied Ocean Research, 56, 48-66. http://dx.doi.org/10.1016/j.apor.2016.01.007.

Thomsen, F., Mendes, S., Bertucci, F., Breitzke, M., Ciappi, E., Cresci, A. Debusschere, E., Ducatel, C., Folegot, F., Juretzek, C., Lam, F-P., O' Brien, J., dos Santos, M. E. (2021) 'Addressing underwater noise in Europe: Current state of knowledge and future priorities.' Kellett, P., van den Brand, R., Alexander, B., Muniz Piniella, A., Rodriguez Perez, A., van Elslander, J., Heymans, J. J. [Eds.] Future Science Brief 7 of the European Marine Board, Ostend, Belgium. http://dx.doi.org/10.5281/zenodo.5534224.

Traverso, F., Gaggero, T., Tani, G., Rizzuto, E., Trucco, A. and Viviani, M. (2017) Parametric analysis of ship noise spectra. IEEE Journal of Oceanic Engineering, 42, 424-438. http://dx.doi.org/10.1109/JOE.2016.2583798.

21st ITTC Cavitation Committee (1996). 'Final Report and Recommendations to the 21st ITTC'. Proceedings of the International Towing Tank Conference.

Vaz, G. (2005) 'Modelling of sheet cavitation on hydrofoils and marine propellers using boundary element methods', PhD thesis, Instituto Superior Técnico, Lisbon, Portugal.

Vaz, G., Bosschers, J. (2006). 'Modeling three dimensional sheet cavitation on marine propellers using a boundary element method'. Proceedings of the 6th International Symposium on Cavitation, Wageningen, the Netherlands.

Vaz, G., Hally, D., Huuva, T., Bulten, N., Muller, P., Becchi, P., Herrer, J.L.R., Whitworth, S., Mace, R., Korsstrom, A. (2015) Cavitating flow calculations for the E779A propeller in open water and behind conditions: code comparison and solution validation, in: Proceedings of the 4th International Symposium on Marine Propulsors, Austin, USA. pp. 330–345.